

Received July 13, 2021, accepted July 29, 2021, date of publication August 5, 2021, date of current version August 11, 2021.

Digital Object Identifier 10.1109/ACCESS.2021.3102830

Failure Analysis of Aluminum Wire Bonds in Automotive Pressure Sensors in Thermal Shock Environments

JUN YANG^{1,2}, PANPAN ZHENG², XIAOGANG LIU², QINGLIN SONG³, YINGFENG ZHU³, BIN SONG², XIAOPING WANG¹, AND SHENG LIU^{1,2,3,4}

¹School of Mechanical Science and Engineering, Huazhong University of Science and Technology, Wuhan 430074, China

²Wuhan FineMEMS Microelectronics Inc., Wuhan 430075, China

³Center of Electronic Manufacturing and Packaging Integration, Institute of Technological Sciences, Wuhan University, Wuhan 430072, China

⁴Laboratory for Hydropower Transients of Ministry of Education, School of Power and Mechanical Engineering, Wuhan University, Wuhan 430072, China

Corresponding author: Sheng Liu (victor_liu63@vip.126.com)

This work was supported by Hubei Provincial Major Program of Technological Innovation under Grant 2017AAA121.

ABSTRACT Wire bonding remains one of the most widely adopted interconnection techniques in the field of electronic packaging. At present, the most effective way to ensure a long life and high reliability of wire bonds is to improve the bonding quality. In this study, both experiments and finite element analysis (FEA) were employed to develop a fundamental understanding of wire bond degradation. Sensors with two protective silicone gels were loaded with the same thermal shock at a temperature ranging from -40°C to 125°C , and the switching time was shorter than 10 s. The number of thermal shock cycles for the aluminum wire covered with transparent silicone reached 1200, but the maximum number of cycles for the other wire only reached 454. The experimental results indicated that the chosen transparent silicone performed better than did the black silicone originally selected, which was also verified by the simulation results. In addition, bond pull and shear tests were performed. The results revealed no degradation of either the Ag-Al or Ni-Al bonding joints under thermal loading. In summary, the root cause of failure was found to be improper protection silicone application, which, as often ignored in analysis, accelerated thermal fatigue of the aluminum wires. An explanation of the observed trend and a recommended aluminum wire bonding method were also provided.

INDEX TERMS Wire bonding, finite element analysis (FEA), pressure sensor, reliability.

I. INTRODUCTION

Wire bonding is a kind of bonding method that relies on thin metal wires and applies heat, pressure and ultrasonic energy to ensure a close bond between metal leads and base plate welding pads to realize electrical interconnection between a given chip and base plate and signal communication between chips [1]–[5]. Failure of wire bonds in microelectronic components in practice has been found to be attributed to the excessive formation of intermetallic compounds (IMCs), oxidation, corrosion, fatigue and electromigration [2]–[7]. These failures occur throughout the lifetime of these components or systems, including manufacturing, testing, storage and operation [6], [7], often resulting in interface separation or cracking [8], [9]. At present, the most effective way to ensure a long

life and high reliability of bonding is to improve the bonding quality [10], which depends on the initial processing window parameters of bonding, such as power, pressure, time, temperature, and selection of wire and bonding pad materials. Typically, bonding pull and shear tests are employed to evaluate the bonding quality [1], [12], [13]. Reliability evaluation has mainly been based on MIL-STD-883 [14] and AEC-Q100 [15] in regard to automotive electronics.

Aluminum wires are widely implemented in interconnections between the module substrate and housing in automotive pressure sensors [1], [12]. Regarding sensors, ensuring the reliability of aluminum wire bonding in harsh environments is a great challenge for researchers and engineers. The higher the reliability of a given product, the more successful it is in the market. In terms of bonding failure, many researchers and engineers have proposed various empirical equations to predict the fatigue life and crack propagation of interfaces and

The associate editor coordinating the review of this manuscript and approving it for publication was Koneru Ramakrishna ¹.

studied the bonding process, including equipment principles, tooling, and processing window parameters [17]–[21], [24].

However, failure analysis and research on aluminum bond wires related to protection glue assembly methods have rarely been reported in regard to automotive pressure sensors. Protection in general is applied in almost all microelectronics-related industries, and this approach is commonly adopted for moisture and dust protection purposes. It is also necessary to protect automotive pressure sensors against moisture intrusion due to the respiration effect [22], even though high-grade waterproof connectors are common. The type of protection glue and thermal fatigue stress issues have mostly been ignored, which could be critical to guarantee the reliability of wire connections. Thermal fatigue-related failure occurs due to unmatched materials and structures under the poor working conditions of road vehicles.

In this paper, we focused on the development of protection glue assembly designs in automotive pressure sensors. There are already approximately 22 applications in both commercial vehicles and passenger cars. It has experienced a notable increase since the early 2000s, when only 14 applications were reported [23]. In this research, we employed both finite element simulations [24] and experiments, conducted a comparative analysis of protective adhesives in our designs, and investigated the root cause of failure. The simulation results agreed well with the experimental results and could provide a positive guiding effect on the design and manufacture of automotive sensors.

II. STRUCTURE, MATERIALS AND METHOD

A. STRUCTURE AND SPECIMENS

The specimens included dual pressure sensors that instantly transformed two independent pneumatic pressure signals in the air reservoirs of brake systems into two independent voltage signals at their terminal pins. The two sensors consist of a measuring cell for calibration and temperature compensation features and aluminum wires providing signal interconnection. Fig. 1 (a) shows the structure of the pressure sensor applied in commercial vehicles. An image of a failed sensor (Fig. 1 (b)) is also provided.

B. EXPERIMENTS AND ELECTRICAL MEASUREMENTS

As pressure sensors are applied to control and monitor the brake system of commercial vehicles, the experiments were based on IEC 60068-2-14 [25]. This standard provides a test platform to verify the ability of components, equipment or other articles to withstand rapid changes in ambient temperature. The test is accelerated because the number of severe changes in temperature during a given period is larger than that under field conditions. The test parameters include high and low temperatures, exposure duration, transfer time or rate of change and number of test cycles. Each specimen should be visually inspected and electrically and mechanically assessed, as required by the relevant specification. The test procedure involves first placing specimens in the

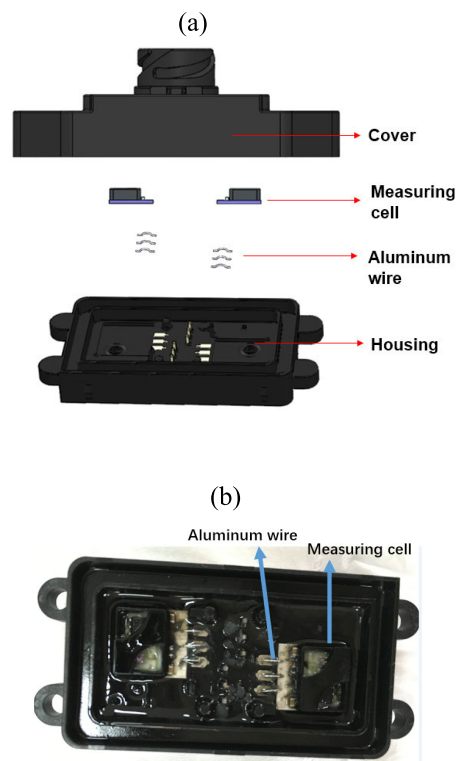


FIGURE 1. In-service failed sensor assembly: (a) structure of the pressure sensor, (b) failed sensor.

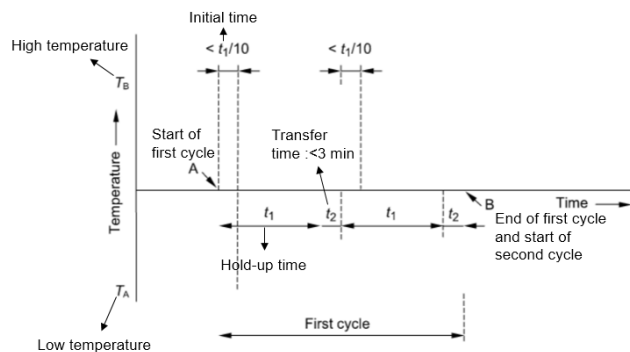


FIGURE 2. Test cycles based on IEC 60068-2-14.

testing chamber, which can maintain the appropriate temperature. Then, we set the test parameters as mentioned above. Fig. 2 shows the test cycles. Finally, the specimens should be recovered under standard atmospheric conditions for testing.

A thermal shock experiment was designed to verify the reliability of the tested sensors. The temperature ranged from T_{min} ($-40^{\circ}C$) to T_{max} ($125^{\circ}C$), the hold time of the two temperature points was 30 minutes, and the switching time was shorter than 10 s. The number of cycles was 500. The sensors were kept in a powered temperature chamber, and signals were continuously monitored during the whole test process. The test profile and actual temperature profile are shown in Fig. 3 (a) and Fig. 3 (b), respectively, and the test facility is shown in Fig. 3 (c).

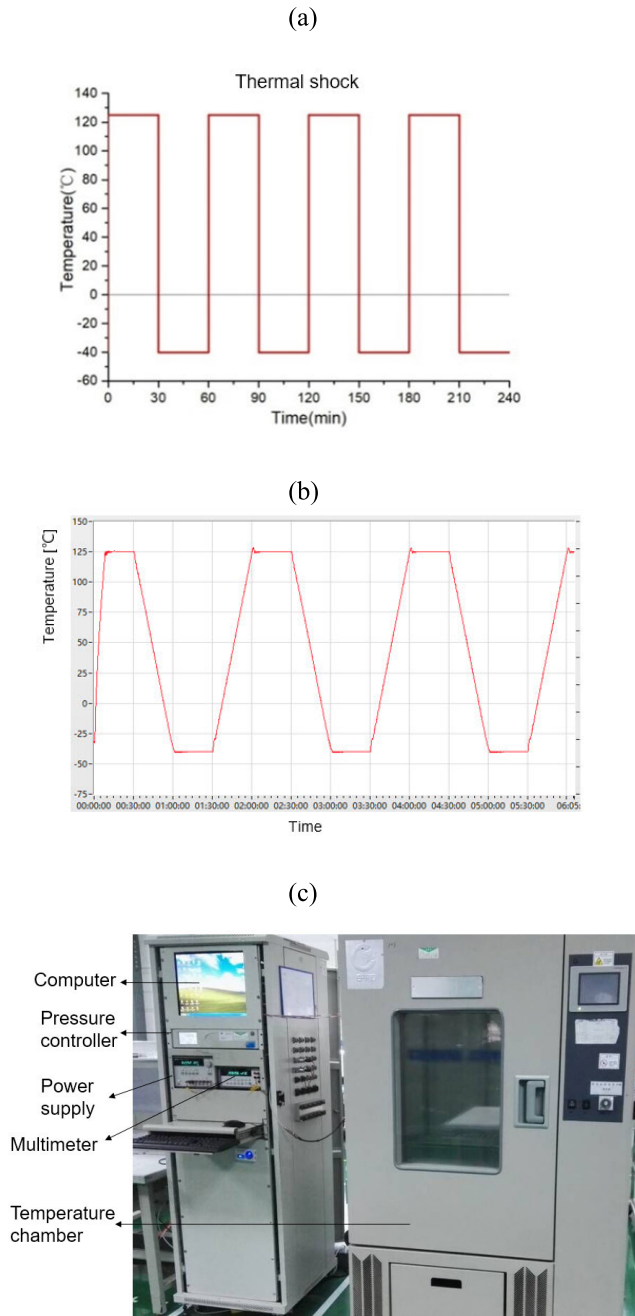


FIGURE 3. Test platform: (a) test profile, (b) actual measuring profile, and (c) test facility.

In this study, 10 sensors with two types of protection glues suitable for aluminum wire bonding were prepared. Five sensors, 15455_BS007-BS011, were protected by black glue (silicone A), and the remaining sensors, 15442_BS001-BS005, were protected by transparent glue (silicone B), as shown in Fig. 4.

Electrical signal measurements were performed during the thermal shock test, and the data are listed in Table 1 and Fig. 5. The electrical output signals of the samples were continuously monitored with a multimeter throughout the whole thermal shock test. The sensors were powered by

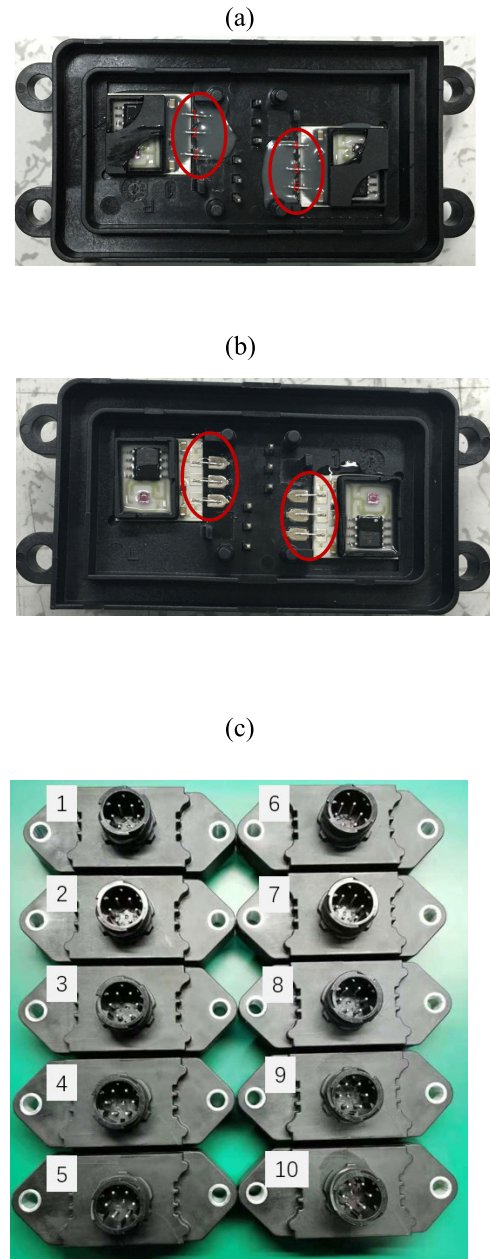


FIGURE 4. Two types of sensor assemblies: (a) black protection glue, (b) transparent protection glue, and (c) test specimens.

a 5-V DC current, and the expected output ranged from 0.9~1.10 V. The sensors have a diagnostic function, namely, when the internal electrical joint is open, the output reaches < 0.5 V or >4.5 V. The required test cycles are 500. As indicated in Table 1, the “sensor #” item indicates the digital number of the specimens, which facilitates convenient identification, and the “sensor name” item indicates the specimen name. The “signal # 21” and “signal # 22” items denote the output signals of the specimens because each specimen provides 2 signal outputs. The “signal during thermal shock test #21/22” item denotes the test result of the two output signals during the thermal shock test. The “status of Al wire #21/22” item indicates the mechanical test result.

TABLE 1. Test results of the functional and mechanical tests.

Sensor #	Sensor name	Electrical result			Mechanical result
		Signal # 21	Signal # 22	Signal during thermal shock test #21/22	Status of Al wire #21/22
1	15442_BS001	AD10	AD09	Passed/Passed	Good/Good
2	15442_BS002	AD15	AD16	Passed/Passed	Good/Good
3	15442_BS003	AD19	AD20	Passed/Passed	Good/Good d
4	15442_BS004	AD08	AD07	Passed/Passed	Good/Good
5	15442_BS005	AD17	AD18	Passed/Passed	Good/Good d
6	15455_BS007	AD22	AD21	Failed/Failed	Failed/Failed
7	15455_BS008	AD23	AD24	Failed/Passed	Failed/Good
8	15455_BS009	AD14	AD13	Passed/Failed	Good/Failed
9	15455_BS010	AD12	AD11	Passed/Failed	Good/Failed
10	15455_BS011	AD04	AD03	Failed/Failed	Failed/Failed

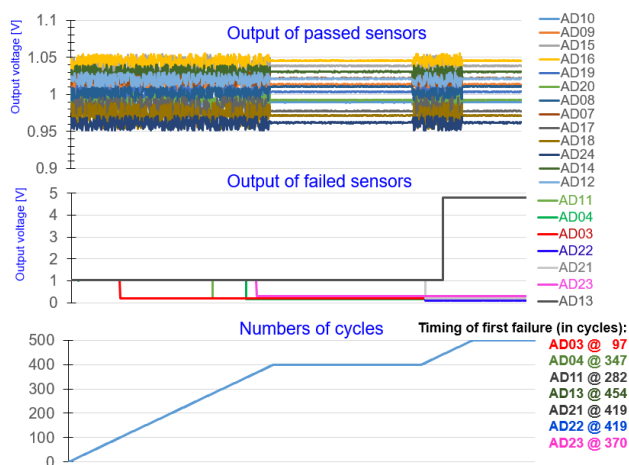


FIGURE 5. Timing of failure in the cycles.

Five specimens, namely, 15442_BS001-15442_BS005, exhibited no failure after the thermal shock test. The other 5 specimens, namely, 15442_BS007-15442_BS011, failed after the test. Fig. 4 shows details of the sensors with and without failure after the thermal shock test. We conducted the test in 2 steps. The first 400 cycles were completed in the first step, and the remaining 100 cycles were completed in the second step. The cycles for the failed specimens ranged from 97 to 454. The minimum number of cycles reached only 97, revealing the poorer protection ability of the black glue than that of the transparent glue.

C. MEASUREMENTS AND SEM OBSERVATION

To identify the failure mode of the sensors, bonding wire pull tests and shear tests were first performed according to MIL-STD-883 [13] and JESD 22B116B (April 2017) [14]. These two standards are the most prevalent and important tests to evaluate the reliability of wire bonding. Fig. 6 shows the results for the 10 specimens and 2 unaged specimens. In each part, there are 6 wires, so there are 6 pull force values and 12 shear force values. The criteria for the bond pull force and shear force indicate that these two forces at failure must be higher than 140 grams and 600 grams, respectively.

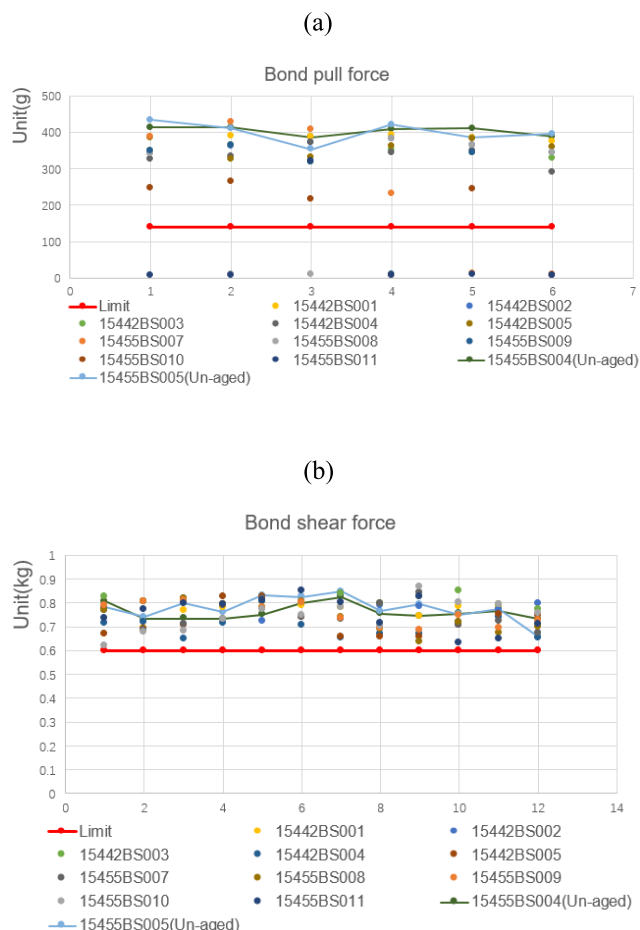


FIGURE 6. Test results: (a) bond pull force test, (b) bond shear force test.

Optical inspection and scanning electron microscopy (SEM) were employed to observe the damaged aluminum wires, as shown in Fig. 7. The failure mode of the specimens was Al wire breakage at the neck position of the first bonding joint. To better observe the specimen microstructure, the protective silicone gel was removed from the bonding wires with a solvent.

D. FEA MODELS

Since assembled components are subject to high road environment loads in vehicles, aluminum bond wires comprise the electrical connection of choice. As shown in Fig. 8, bond wires connected adjacent contact pads, with one wire at the ceramic substrate and the other at the pin in plastic housing. As a consequence, these wires were bent in an arch shape. The ceramic substrate was affixed onto the housing with a specific silicone. The silicone material is a one-part, gray adhesive with a high tensile strength, and the thickness is 50 μm based on the measurement result. Fig. 8 also shows the detailed model of this bond wire. The wire was affixed via wedge bonds on both sides. In this case, the bond wire was a Heraeus ALW-49P, with a thickness of 300 μm, consisting of high-purity Al. The density of Al was 2.7 g/cm³,

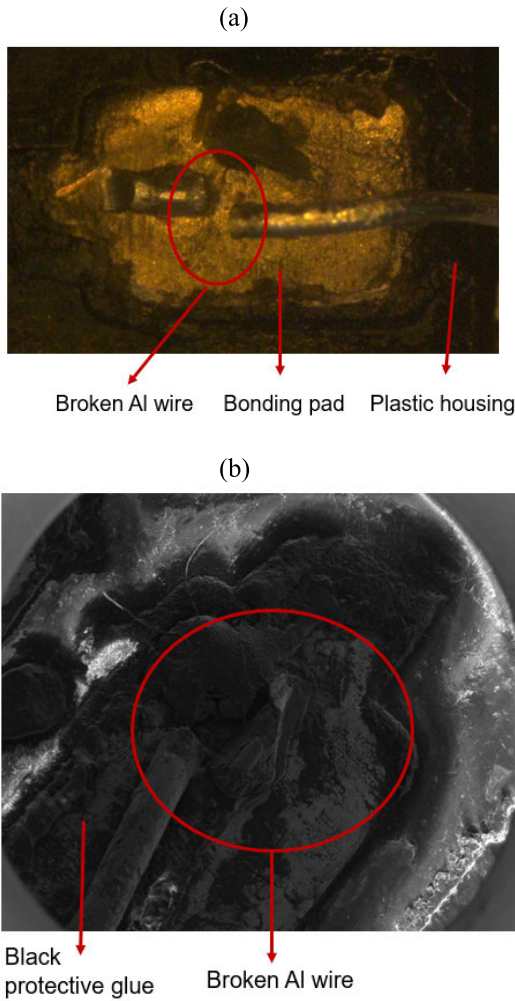


FIGURE 7. (a) Optical inspection and (b) SEM images of the failed Al wire.

the Poisson's ratio was 0.33 and the Young's modulus was 70.0 GPa. Given the same symmetrical structure, the aluminum wire was simplified and modeled with ANSYS software [28], and the detailed dimensions of the Cu-Ni-Al joint are listed in Table 2. To investigate the behavior of the aluminum bond wires in a thermal shock-loaded environment, first, wire shape stress analysis was performed. Next, the performance of the bond wires covered with the 2 types of silicone were analyzed. Both silicone cuboids were assumed to exhibit two shapes: one shape was an overall arch with a height of 1.6 mm, a width of 1.6 mm and a length of 5.5 mm (as shown in Fig. 9 (a)), and the other shape was a half bridge with a height of 1.2 mm, a width of 1.6 mm and a length of 2.5 mm (please refer to Fig. 9 (b)).

The material data were obtained from the suppliers and some of their properties were tested in house and are listed [29], [30]. The glass transition temperature of the silicone A and silicone B is -55°C and -60°C respectively. The constitutive models adopted were established as follows: regarding the metallic materials involved, constitutive models

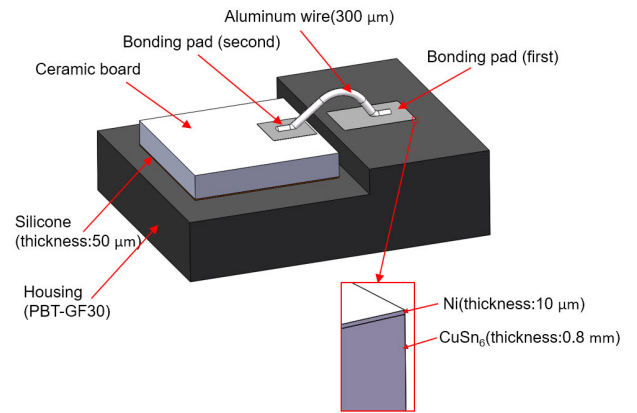


FIGURE 8. Simplified FE model: aluminum wire bonding of the pressure sensor.

TABLE 2. Detailed dimensions.

Item	Dimensions (mm)
Bonding pad (second)	1.81*1.81*0.013
Ceramic board	6*6*1
Bonding pad (first)	3*2*0.01
CuSn6	3*2*0.8
PBT-GF30	12.5*10
Aluminum wire diameter	0.3
Fully covered silicone	1.6*5.5*1.6
Partly covered silicone	1.6*2.5*1.2

TABLE 3. Major properties of the materials [29], [30].

Material	Density (g/cm ³)	E (GPa)	ν	CTE (10 ⁻⁶ /°C)	Thermal Conductivity (W/m·K)	Yield Strength (MPa)
CuSn6	8.83	110	0.3	17.2	98	400
Ni	8.8	201	0.31	9.2	90.7	59
Al	2.7	70	0.33	23.6	247	20
Ag	11	71	0.37	20	420	35
Al ₂ O ₃	3.7	300	0.26	6.5	21	69
PBT-GF30	1.53	9.8	0.39	25	0.27	46
Silicone A	1.29	0.01	0.48	350	0.2	-
Silicone B	0.95	6×10^{-5}	0.49	335	0.195	-

of bilinear isotropic hardening behavior were assumed (Al, Ni, Ag, and CuSn6). The other materials were assumed to be linear elastic. Regarding plastic or polymer films, only thermoelasticity behavior was assumed due to the small thickness of the silicone films. More robust constitutive models will be used in future work, which will require notable testing work to obtain rate- and temperature-dependent material properties.

Mesh dependence was checked for comparison, as shown in Table 4. It shows that the error between the maximum strain value of the simulation in this study and that of the simulation with refine grid is only 1.26%, which is acceptable.

The numerical solution from finite element model and the measurement results of actual sample were analyzed and compared in order to prove the validation of the established FEA model. The result of the force-displacement curve was obtained by solving for the reaction force. Fig. 10(a) shows the FEA result of pull force of aluminum wire, Fig.10(b)

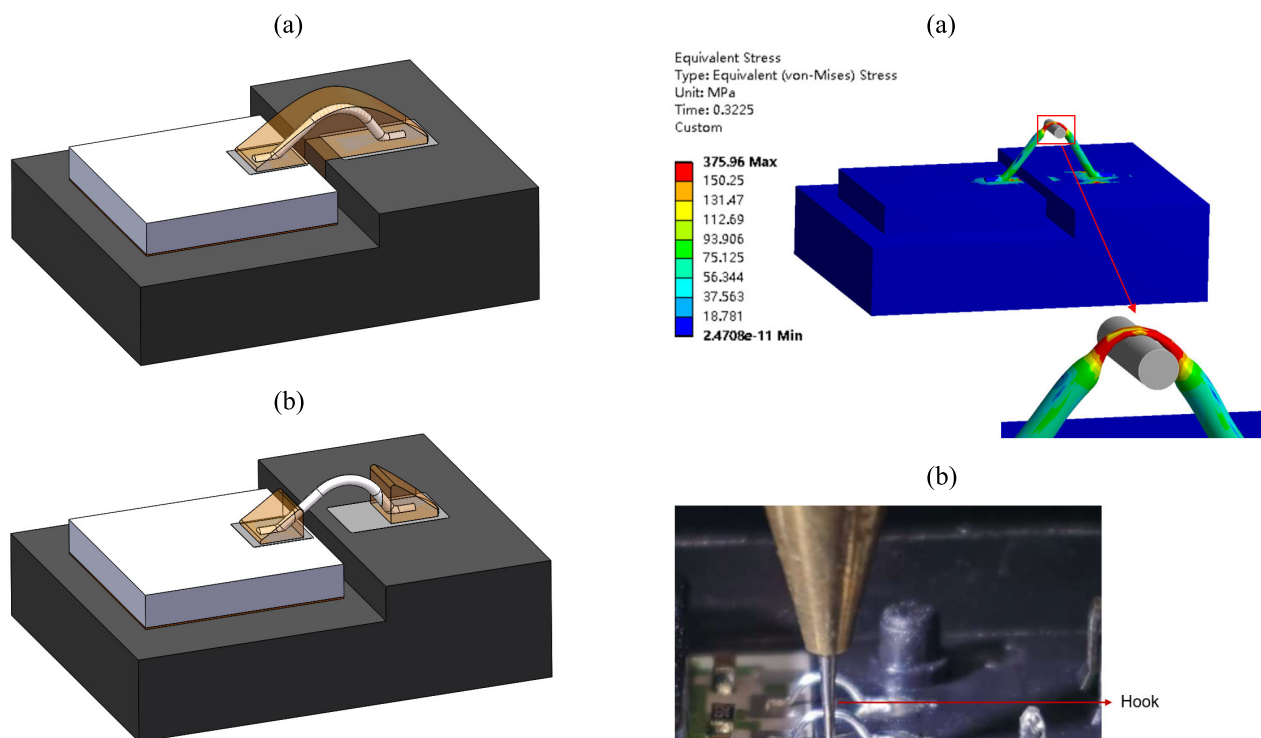


FIGURE 9. Assumed FE models of silicone cuboids: (a) fully covered aluminum wire and (b) partially covered aluminum wire.

TABLE 4. Influence of mesh effect.

Model	Medium mesh	Fine mesh	Error
Number of elements	12451	103105	--
Minimum element size(mm)	1.98×10 ⁻³ mm	1.06×10 ⁻³ mm	--
Maximum strain	0.008397	0.008503	1.26%

shows the actual test sample and measuring equipment, and Fig. 10(c) presents the comparison of simulation results and experimental measurement results, from which it can be found that the actual experimental test results are consistent well with the simulation results. Therefore, the validation of the FEA model was proven.

III. RESULTS AND DISCUSSION

A. VISUAL INSPECTION AND SEM OBSERVATION OF ALUMINUM WIRE BONDS

Fig. 11 shows the bonding surface after the shear test. Fig. 11 (a) shows the bonding surface of the ceramic board pad, and Fig. 11 (b) shows the bonding surface of the pins in the housing. As described in section 2.3 regarding the test data, the 5 failed parts resulted in the same failure mode, i.e., wire neck fracture, under a pull force lower than 50 g. However, the shear force still met the requirements for solid metallurgical bonds at the interface. This indicated that the bond strength of the aluminum wires degraded after thermal

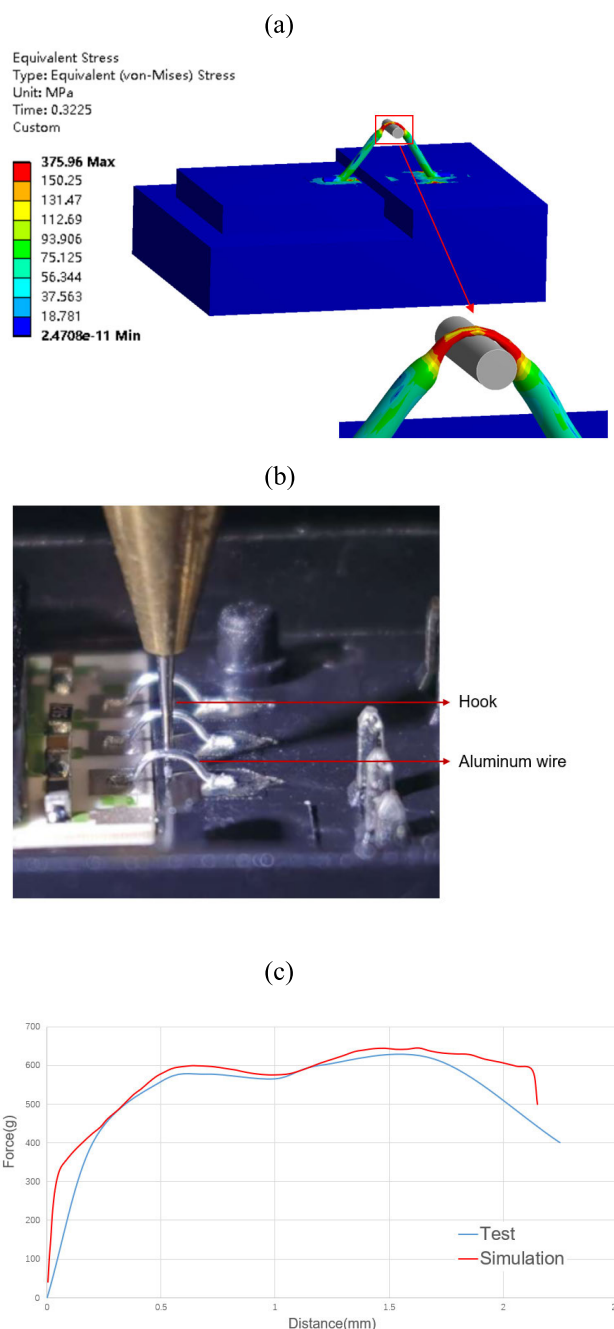


FIGURE 10. Validation of FEA model: (a) FEA result of pull force of aluminum wire, (b) actual test equipment, (c) compared result of test and simulation.

aging with improper protective glue, and the applied glue accelerated the degradation process and yielded a reduced reliability.

B. EFFECTS OF THE PROTECTION SILICONES

Figs. 12 (a) and (b) show the equivalent plastic strain in the aluminum wire with the different finite element models. There was no major difference between the results of these two models. Both models show the maximum plastic strain

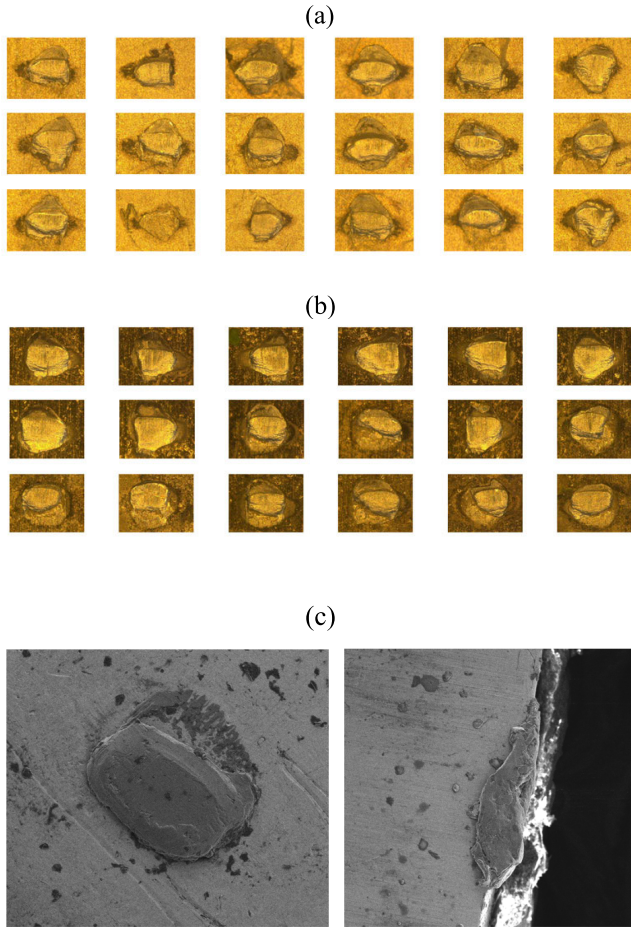


FIGURE 11. Bonding surfaces: (a) bonding pads of the ceramic board, (b) bonding pads of the pins in the housing, (c) SEM images of the front and cross section of the bonding pad of the failed aluminum wire.

occurred at the neck of the bonding wire. It was the same position as in the failure of the experimental results. However, for a different type of silicone, the results for the maximum plastic strain at the neck of the aluminum wire with silicone A indicated a value up to 0.024196, while the maximum plastic strain with silicone B indicated a value of 0.0076436. The results were summarized in the Table 5. This occurred because of the different CTE and E values of the adjacent materials. The silicone A was hard after curing and the silicone B was soft after curing. The hard glue had a large stress on the aluminum wire under the thermal shock test, while the soft glue had a small stress on the aluminum wire. With the test time increased, the accumulated plastic strain tended to increase, which would eventually cause the corresponding failure.

C. EFFECTS OF THE SILICONE MATERIALS ON THE THERMAL FATIGUE LIFE

Table 5 summarizes the FEA results of the fatigue life regarding the effects of the adopted silicone on the bond reliability under thermal shock loading, which is based on

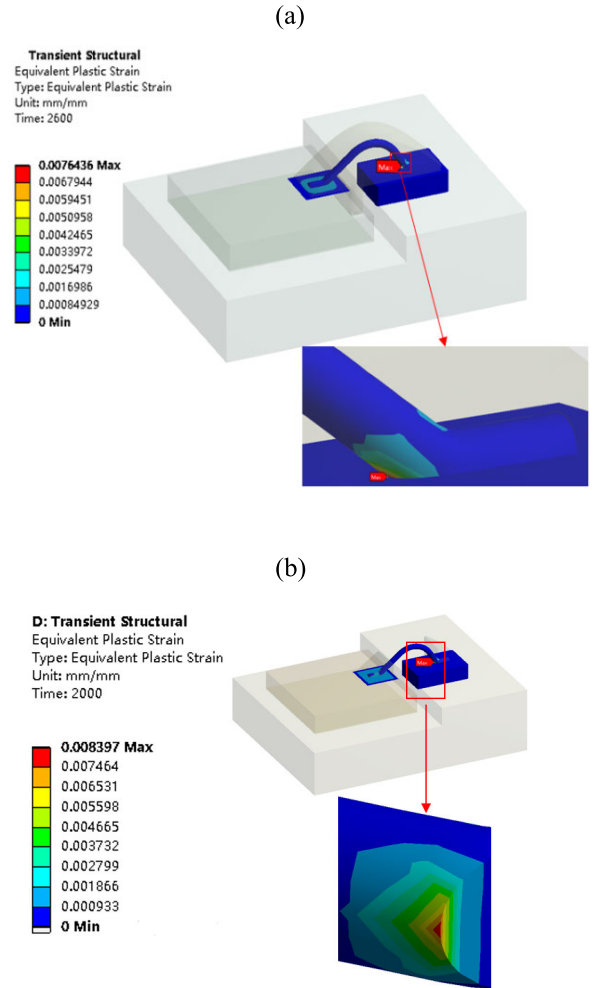


FIGURE 12. FEA results for the both models.

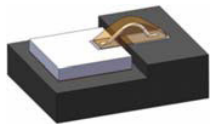
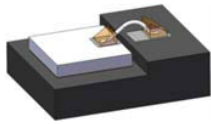
the Coffin-Manson model. The cycles of fatigue life can be calculated under the condition of the effective bonding plastic strain with the following equation:

$$N_f = 0.5(\Delta\gamma/2\varepsilon_f)^{1/C}$$

where N_f is the mean number of cycles to failure, $\Delta\gamma$ is the bonding plastic strain, ε_f is the fatigue ductility coefficient and C is the fatigue ductility exponent. In this study, ε_f was set to 3.09, and C was set to 0.673 [11]–[13]. The FEA results obtained with the 2 models considering different coating structures are listed below. Cases 1 and 2 involved the FE models with silicone covering.

The predicted lifetime for silicone A (black silicone) was 834 cycles, compared to the predicted lifetime of 4623 cycles for silicone B (transparent silicone). The fatigue life of the silicone A partial coating model was predicted to be longer than that predicted with the full coating model. It was obvious that the adopted silicone with a lower E value resulted in a longer fatigue life of the aluminum wire. This was highly consistent with the experimental results. The aluminum wires

TABLE 5. Summary of the FEA results of the fatigue life.

Item	Structure	Silicone	Maximum Plastic Strain	Cycles of Fatigue Life
1		Silicone B	0.0076436	4623
		Silicone A	0.024196	834
2		Silicone B	0.008397	4020
		Silicone A	0.013879	1905

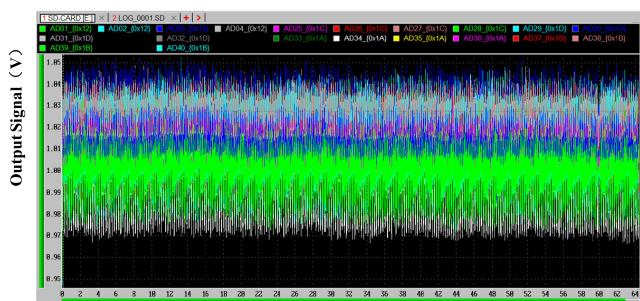


FIGURE 13. Output results of the pressure sensors.

covered with black silicone all failed and exhibited the same failure mode of neck fracture. The minimum number of failure cycles was only 97, and the maximum number of failure cycles was 454. The aluminum wires covered with transparent silicone, however, remained intact with a high reliability, and the number of thermal shock cycles reached up to 1200. No mechanical nor electrical signal failures were observed. The output voltage test results are shown in Fig. 13. The test results of the 10 improved sensors covered with transparent protective glue are shown. The thermal shock test was repeated and completed on the customer side. A total of 1200 cycles was conducted, far more than the engineering requirements. The signal output remained suitable throughout the whole test. This trend is consistent with the simulation results, but we could not perform more cycles because the test cost associated with the completion of 4623 cycles was extremely high.

IV. CONCLUSION

The root cause of aluminum wire failure was investigated via visual inspection, SEM observation, design of experiments (DOE) test, and numerical DOE modeling experiments. It was concluded that the improper protective silicone covering the aluminum wire led to a reduction in sensor life. This suggested that an unmatched glue with an unsuitable

CTE value accelerated the thermal fatigue process of aluminum wire under thermal shock loading. The axial loading was very high and exceeded the axial tension value, and the degree of forced elongation of the Al wire in the process of expansion and contraction resulted in wire fracture. In addition, the shear force test results after thermal shock testing were very close to the shear force results of unaged bonds. In particular, no apparent degradation of the bonding point was observed. This demonstrated that the shear force, as tested based on bonding qualification, is not a necessary condition but a sufficient condition. The pull force test is a necessary test in mass production.

The preliminary FE simulation results supported the experimental results of aluminum wire bonding under thermal shock loading, which indicated that virtual testing modeling could facilitate large-scale production of highly sensitive sensors.

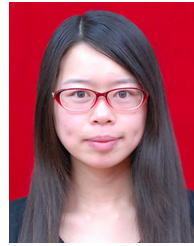
ACKNOWLEDGMENT

Part of this work was performed within a research project at Wuhan FineMEMS Inc. The pull and shear tests and electric tests were conducted with the assistance of the Department of Research of FineMEMS.

REFERENCES

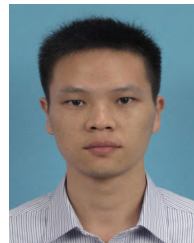
- [1] S. Manoharan, C. Patel, S. Hunter, and P. McCluskey, "Mechanism of wire bond shear testing," *Microelectron. Rel.*, vols. 88–90, pp. 738–744, Sep. 2018.
- [2] M. Petzold, L. Berthold, D. Katzer, H. Knoll, D. Memhard, P. Meier, and K.-D. Lang, "Surface oxide films on aluminum bondpads: Influence on thermosonic wire bonding behavior and hardness," *Microelectron. Rel.*, vol. 40, nos. 8–10, pp. 1515–1520, Aug. 2000.
- [3] H. Xu, C. Liu, V. V. Silberschmidt, and Z. Chen, "Growth of intermetallic compounds in thermosonic copper wire bonding on aluminum metallization," *J. Electron. Mater.*, vol. 39, no. 1, pp. 124–131, Jan. 2010.
- [4] T. J. S. Anand, C. K. Yau, and L. B. Huat, "Oxidation study on as-bonded intermetallic of copper wire–aluminum bond pad metallization for electronic microchip," *Mater. Chem. Phys.*, vol. 136, nos. 2–3, pp. 638–647, 2012.
- [5] J. E. Krzanowski and N. Murdeshwar, "Deformation and bonding processes in aluminum ultrasonic wire wedge bonding," *J. Electron. Mater.*, vol. 19, no. 9, pp. 919–928, Sep. 1990.
- [6] I. Lum, M. Mayer, and Y. Zhou, "Footprint study of ultrasonic wedge-bonding with aluminum wire on copper substrate," *J. Electron. Mater.*, vol. 35, no. 3, pp. 433–442, 2006.
- [7] C. M. Tan and Z. Gan, "Failure mechanisms of aluminum bondpad peeling during thermosonic bonding," *IEEE Trans. Device Mater. Rel.*, vol. 3, no. 2, pp. 44–50, Jun. 2003.
- [8] L. Merklet, M. Sonner, and M. Petzold, "Lifetime prediction of thick aluminium wire bonds for mechanical cyclic loads," *Microelectron. Rel.*, vol. 54, no. 2, pp. 417–424, 2014.
- [9] S. Ramminger, P. Türkes, and G. Wachutka, "Crack mechanism in wire bonding joints," *Microelectron. Rel.*, vol. 38, nos. 6–8, pp. 1301–1305, Jun. 1998.
- [10] S. Ramminger, N. Seliger, and G. Wachutka, "Reliability model for al wire bonds subjected to heel crack failures," *Microelectron. Rel.*, vol. 40, nos. 8–10, pp. 1521–1525, Aug. 2000.
- [11] A. S. Bahman, F. Iannuzzo, T. Holmgaard, R. Nielsen, and F. Blaabjerg, "Reliability-oriented environmental thermal stress analysis of fuses in power electronics," *Microelectron. Rel.*, vols. 76–77, pp. 25–30, Sep. 2017.
- [12] M. S. Broll, U. Geissler, J. Höfer, S. Schmitz, O. Wittler, and K. D. Lang, "Microstructural evolution of ultrasonic-bonded aluminum wires," *Microelectron. Rel.*, vol. 55, no. 6, pp. 961–968, May 2015.
- [13] Department of Defense Standard, *Test Method Standard Microcircuits*, Standard US.MIL-STD-883K, Feb. 2017.

- [14] *Wire Bond Shear Test Method*, J. E. D. E. C. Standard JESD22-B116B, JEDEC Solid State Technology Association, Apr. 2017.
- [15] AEC Standard, *Wire Bond Shear Test. Automotive Electronics Council Component Technical Committee*, Standard AEC-Q100-001, Sep. 2014.
- [16] T. J. S. Anand, C. Kok Yau, and A. Jalar, "Micro-structural studies of thermosonic Cu-Al bonding interface," *Adv. Mater. Res.*, vol. 925, pp. 154–158, Apr. 2014.
- [17] L. Maiocco, D. Snyers, P. R. Munroe, and I. Baker, "Correlation between electrical resistance and microstructure in gold wirebonds on aluminum films," *IEEE Trans. Compon., Hybrids, Manuf. Technol.*, vol. 13, no. 3, pp. 592–595, Sep. 1990.
- [18] O. Schilling, M. Schäfer, K. Mainka, M. Thoben, and F. Sauerland, "Power cycling testing and FE modelling focussed on Al wire bond fatigue in high power IGBT modules," *Microelectron. Rel.*, vol. 52, nos. 9–10, pp. 2347–2352, Sep. 2012.
- [19] S. Manoharan, C. Patel, P. McCluskey, and M. Pecht, "Effective decapsulation of copper wire-bonded microelectronic devices for reliability assessment," *Microelectron. Rel.*, vol. 84, pp. 197–207, May 2018.
- [20] T. Y. Hung, S. Y. Chiang, C. J. Huang, C. C. Lee, and K. N. Chiang, "Thermal-mechanical behavior of the bonding wire for a power module subjected to the power cycling test," *Microelectron. Rel.*, vol. 51, nos. 9–11, pp. 1819–1823, 2011.
- [21] A. J. G. Strandjord, S. Popelar, and C. Jauernig, "Interconnecting to aluminum- and copper-based semiconductors (electroless-nickel/gold for solder bumping and wire bonding)," *Microelectron. Rel.*, vol. 42, no. 2, pp. 265–283, Feb. 2002.
- [22] G. F. Gong, "The research on respiration effect," *Radar Sci. Technol.*, vol. 7, no. 3, pp. 236–244, Jun. 2009.
- [23] C.Y. Wei, *Bosch Automotive Handbook*, 3rd ed. Beijing, China: Beijing Institute of Technology Press, Apr. 2009.
- [24] S. Liu and Y. Liu, *Modeling and Simulation for Microelectronic Packaging Assembly*. Hoboken, NJ, USA: Wiley, 2012.
- [25] International Standard, *Environmental Testing—Part 2-14: Tests—Test N; Change of Temperature. International Electrotechnical Commission, Edition 6.0*, Standard IEC 60068-2-14, Jan. 2009.
- [26] N. V. Chidambaram, "A numerical and experimental study of temperature cycle wire bond failure," in *Proc. 41st Electron. Compon. Technol. Conf.*, May 1991, pp. 877–882.
- [27] *Heraeus ALW-49P*. Accessed: Mar. 16, 2021. [Online]. Available: <https://www.heraeus.com>
- [28] *ANSYS Mechanical User Guide*, Release 14.5, ANSYS, Canonsburg, PA, USA, Oct. 2012.
- [29] L. Xu, M. Wang, Y. Zhou, Z. Qian, and S. Liu, "Effect of silicone gel on the reliability of heavy aluminum wire bond for power module during thermal cycling test," in *Proc. IEEE 66th Electron. Compon. Technol. Conf. (ECTC)*, May 2016, pp. 1005–1010.
- [30] Y. Q. Guo, T. Gao, Y. J. Xu, L. H. Liang, and Y. Liu, "Life prediction of bonding interface in power module under thermal cycling loading," *J. Mech. Elect. Eng.*, vol. 35, no. 1, pp. 73–78, 2017.



PANPAN ZHENG was born in Kaifeng, Henan, China, in 1988. He received the B.S. degree in mechanical engineering and automation from Zhengzhou University, in 2012, and the M.A. degree in precision measurement physics from Huazhong University of Science and Technology, in 2016.

From 2019 to 2020, he has focused on the CAE for pressure sensors at Wuhan Finemems Inc.



XIAOGANG LIU was born in Jingzhou, Hubei, China, in 1987. He received the B.S. and M.A. degrees in mechanics engineering from Huazhong University of Science and Technology, in 2009 and 2019, respectively.

From 2019 to 2020, he has focused on the CAE for pressure sensors at Wuhan Finemems Inc.



QINGLIN SONG graduated from the Institute of Electronics, Chinese Academy of Sciences, in 2004. He has been devoted to the research and development of MEMS, especially sensors for many years. In 2003, he went to Rutherford Laboratory as a Visiting Scholar to participate in the cooperation projects between Chinese Academy of Sciences and Royal Society of Britain, and participated in the research of 863 973, the National Torch Program, and other major projects of the

Ministry of Science and Technology of the People's Republic of China. Since 2004, he has been responsible for the development and industrialization of Goethe micro electromechanical technology microphone, and gradually expanded to other fields of MEMS sensors, such as MEMS temperature, humidity, pressure, gas, and other sensors, and making new contributions to the development of sensor field in China. As the first inventor, he has obtained more than 160 authorized patents (including more than 30 invention patents).



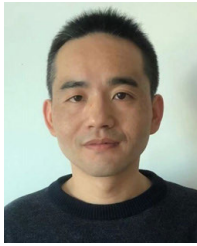
JUN YANG was born in Jingzhou, Hubei, China, in 1983. He received the B.S. degree in electronic information engineering from Huazhong University of Science and Technology, in 2004, where he is currently pursuing the Ph.D. degree in mechanical engineering.

Since 2005, he has been focusing on the design for pressure sensors. He is currently the Project and Development Manager at Wuhan Finemems Inc. More than ten types of pressure sensors had been widely used in vehicles in global market. His research interests include materials, processes, applications, and electronic circuit design.



YINGFENG ZHU was born in Kunming, Yunnan, China, in 1971. He graduated from Tianjin University. He received the Bachelor of Science degree in photo electronics.

Since 1993, he has been focusing on the research and development for infrared dewar and package. Since 2008, he has been the project manager of infrared MW 320 × 256 FPA detector.



BIN SONG was born in Yangxian, Shanxi, China, in 1983. He received the B.S. and M.A. degrees in mechanics engineering from Huazhong University of Science and Technology, in 2005 and 2008, respectively.

Since 2008, he has been focusing on the CAE for pressure sensors at Wuhan Finemems Inc.



XIAOPING WANG received the B.S. and M.A. degrees in control theory and control engineering from Wuhan University of Technology.

He is currently the Chief Executive Officer of Wuhan Finemems Inc. He is leading the design, development, production, and manufacture of automotive sensors. He has authored more than 50 patents on these topics. He won the First Prize of the Science and Technology Award of the Chinese Society of Electronics, in 2018

(Technology Invention Category).



SHENG LIU received the B.S. and M.S. degrees from Nanjing University of Aeronautics and Astronautics, in 1983 and 1986, respectively, and the Ph.D. degree from Stanford University, in 1992.

He is currently a Changjiang Scholar Professor of mechanical engineering at the Huazhong University of Science and Technology and he has a dual appointment at Wuhan National Laboratory for Optoelectronics. He was once a Tenured Faculty at Wayne State University. He has over 18 years' experience in LED/MEMS/IC packaging. He has extensive experience in consulting with many leading multinational and Chinese companies. He was an Aircraft Designer at the Chengdu Aircraft Company for two years. He has filed and owned more than 140 patents in China and in the USA, has published more than 500 technical articles, given more than 100 keynotes and invited talks, and edited more than nine proceedings in English for ASME and IEEE. He is an ASME Fellow. Since 2006, he has been one of the 11 National Committee Member in LED at the Ministry of Science and Technology of China. He won the prestigious White House/NSF Presidential Faculty Fellow Award, in 1995, the ASME Young Engineer Award, in 1996, the NSFC Overseas Young Scientist Award, China, in 1999, the IEEE CPMT Exceptional Technical Achievement Award, in 2009, and the Chinese Electronic Manufacturing and Packaging Technology Society Special Achievement Award, in 2009. He has been an Associate Editor of IEEE TRANSACTIONS ON ELECTRONIC PACKAGING MANUFACTURING, since 1999, and *Frontiers of Optoelectronics in China*, since 2007.

...